

**Letter of Intent for the SNS FnpB**  
**Precision Measurement of Neutron Decay Parameters**

The *abBA* Experiment

J.D. Bowman (Spokesman), W.S. Wilburn (Spokesman), J.M. O'Donnell, and S.I. Penttilä  
*Los Alamos National Laboratory*

J.R. Calarco and F.W. Hersman  
*University of New Hampshire*

T.E. Chupp  
*University of Michigan*

T.V. Cianciolo, K.P. Rykaczewski, and G.R. Young  
*Oak Ridge National Laboratory*

R.T. De Souza and W.M. Snow  
*Indiana University*

E. Frlež and D. Počanić  
*University of Virginia*

T.R. Gentile  
*National Institute of Standards and Technology*

G.L. Greene, and R.K. Grzywacz  
*University of Tennessee*

V. Gudkov  
*University of South Carolina*

G.L. Jones  
*Hamilton College*

G.S. Mitchell  
*University of California, Davis*

P.-N. Seo  
*North Carolina State University*

August 24, 2005

## Abstract

We propose an experiment (the *abBA* experiment) for the SNS FNPB which will determine four neutron decay parameters to greater precision than previous measurements. These parameters are the three time-reversal allowed correlations  $A$  (correlation between electron momentum and neutron spin),  $B$  (correlation between anti-neutrino momentum and neutron spin), and  $a$  (correlation between electron and anti-neutrino momenta), and the Fierz interference term  $b$ . These measurements will provide a redundant determination of  $\lambda = g_A/g_V$ . Previous experiments on determinations of  $\lambda$  in neutron decay have focused on measuring only one parameter, mostly  $A$ . Also these experiments have been limited in precision primarily by two effects: large backgrounds and uncertainty in neutron polarization. The *abBA* approach addresses the first of these limitations by observing coincidences between the decay proton and electron in high-quality silicon detectors, greatly reducing the background. It also decreases the uncertainty in neutron polarization through the use of a polarized  $^3\text{He}$  neutron spin filter which allows precision neutron polarimetry.

# 1 Scientific Motivation

Neutron  $\beta$ -decay provides the most precise measurement of the ratio of axial to vector coupling constants  $\lambda = g_A/g_V$ . The precise value of  $\lambda$  is very important in many applications of the theory of weak interactions, especially in astrophysics, *e.g.* a star's neutrino production is proportional to  $\lambda^2$ . The increasing of experimental accuracy moves neutron decay experiments to a much more fundamental level since precise measurements of neutron  $\beta$ -decay parameters are very important in the search for new physics. For example, since the neutron decay rate is proportional to the square of the Cabibbo-Kobayashi-Maskawa (CKM) matrix element  $V_{ud}$ , we can obtain  $V_{ud}$  (the  $u$  and  $d$  quark mixing matrix) independently of the nuclear model.

Currently, the most accurate value of the matrix element  $V_{ud}$  is obtained from the measurement of nuclear Fermi transitions in  $0^+ \rightarrow 0^+$  nuclear  $\beta$ -decay. However, the procedure of the extraction of this matrix element involves calculations of radiative corrections for the Fermi transition in nuclei. Despite the fact that these calculations have been done with high precision (see [1] and references therein), it is impossible to control the values of these nuclear corrections from independent experiments.

It is expected that the planned measurements of the neutron lifetime [2] and angular coefficients [3] will provide a value for  $V_{ud}$  with an accuracy comparable to or better than the value determined from the  $0^+ \rightarrow 0^+$  nuclear  $\beta$ -decay experiments. The expected increase in the accuracy of experimental data in neutron decay will elevate the status of these experiments and rank them among the most important experiments in fundamental physics.

With a more accurate value for  $V_{ud}$  one could possibly resolve the unitarity problem of the CKM-matrix. The unitarity condition for the CKM matrix in the Standard Model of the electroweak interaction,

$$|V_{ud}|^2 + |V_{us}|^2 + |V_{ub}|^2 = 1, \quad (1)$$

gives a constraint on the three matrix elements. Two of matrix elements,  $V_{us} = 0.2196 \pm 0.0023$  and  $V_{ub} = 0.0036 \pm 0.0007$  [4], have been extracted from high energy physics experiments (see also [5, 6]). The current value of  $V_{ud}$  obtained from nuclear  $0^+ \rightarrow 0^+$  nuclear  $\beta$ -decay is  $0.9740 \pm 0.0005$  [1]. The  $V_{ud}$  value obtained from neutron  $\beta$ -decay is  $0.9713 \pm 0.0014$  [7]. When we use these values and uncertainties in equation 1, there is, at the level of  $10^{-3}$ , room for new physics (see for example [7, 8, 9, 10, 11, 12] and references therein). It has been argued that the deviation from unitarity could be related to uncertainties in determination of the parameter  $V_{us}$  (see, for example, [13, 14]). However, the first element  $V_{ud}$  gives the dominant contribution to the unitarity equation and, therefore, it is crucial to obtain a more precise value of  $V_{ud}$  before we can draw a conclusion about a validity of the Standard Model.

We propose an experiment (the *abBA* experiment [3]) for the SNS FNPB which will determine four neutron decay parameters to greater precision than previous measurements. These parameters are the three time-reversal allowed correlations  $A$  (correlation between electron momentum and neutron spin),  $B$  (correlation between anti-neutrino momentum and neutron spin), and  $a$  (correlation between electron and anti-neutrino momenta), and the Fierz interference term  $b$ . In tree approximation, and neglecting recoil corrections and electron polarization, the neutron decay rate can be described by [15]

$$dW \propto \frac{1}{\tau_n} F(E_e) \left[ 1 + a \frac{\vec{p}_e \cdot \vec{p}_\nu}{E_e E_\nu} + b \frac{m_e}{E_e} + B \frac{\vec{\sigma}_n \cdot \vec{p}_\nu}{E_\nu} + A \frac{\vec{\sigma}_n \cdot \vec{p}_e}{E_e} \right], \quad (2)$$

where  $\vec{p}_e$  and  $\vec{p}_\nu$  are the outgoing electron and neutrino momenta,  $\vec{\sigma}_n$  is the neutron spin, and  $E_\nu$  is the neutrino energy.  $F(E_e)$  is a Fermi function and  $\tau_n$  is the neutron lifetime. It is important to note that both  $A$  and  $B$  are multiplied by  $\vec{\sigma}_n$ , requiring that the neutron polarization be measured to the same precision desired for any determination of  $A$  or  $B$ . In the tree approximation the angular coefficients depend only on one parameter,  $\lambda$  (which can be chosen to be real for time reversal invariant interactions):

$$a = \frac{1 - \lambda^2}{1 + 3\lambda^2}, \quad A = -2\frac{\lambda^2 + \lambda}{1 + 3\lambda^2}, \quad B = 2\frac{\lambda^2 - \lambda}{1 + 3\lambda^2}, \quad (3)$$

and the parameter  $b$  is equal to zero for the standard vector – axial vector type of weak interactions. In these formulas we assume  $\lambda < 0$ .

The three correlations are all sensitive (to a differing degree) to the parameter  $\lambda$ . Combining  $\lambda$  with information from neutron and muon lifetime measurements provides a determination of the  $V_{ud}$  element of the CKM-matrix. It should be noted that even high precision measurements of the  $a$ ,  $A$  and  $B$  coefficients, and the total decay rate cannot result in pure  $\lambda = g_A/g_V$  without unknown radiative corrections both for vector and axial – vector currents. This is because equation (3) is invariant under transformation

$$\lambda \rightarrow \lambda \frac{1 + \frac{\alpha}{2\pi} a_A}{1 + \frac{\alpha}{2\pi} a_V}, \quad (4)$$

where  $a_V$  and  $a_A$  are hadronic structure dependent parts of the radiative corrections for Fermi and Gamow-Teller transitions, respectively (see, for example [16, 17]). This means that we will measure an effective renormalized parameter  $\lambda$ . However, it does not affect the search for new physics and precise definition of  $V_{ud}$  matrix element provided we are using only neutron decay experimental data.

To be able to extract the parameters  $\lambda$  and  $V_{ud}$ , and to search for the possible manifestation of new physics [18], we take into account all recoil and radiative corrections up to the required accuracy ( $10^{-5}$  in our case). These corrections essentially modify the expression for the neutron decay rate. Thus, using, for example, a parametrization based on the effective field theory calculations, the differential neutron decay rate can be written as (see for details [19, 20]):

$$\begin{aligned} \frac{d\Gamma^3}{dE_e d\Omega_{\vec{p}_e} d\Omega_{\vec{p}_\nu}} &= \frac{(G_F V_{ud})^2}{(2\pi)^5} |\vec{p}_e| E_e (E_e^{\max} - E_e)^2 \\ &\times \left\{ C_0(E_e) + \frac{\vec{p}_e \cdot \vec{p}_\nu}{E_e E_\nu} C_1(E_e) + \left[ \left( \frac{\vec{p}_e \cdot \vec{p}_\nu}{E_e E_\nu} \right)^2 - \frac{\beta^2}{3} \right] C_2(E_e) \right. \\ &\left. + \frac{\vec{\sigma}_n \cdot \vec{p}_e}{E_e} C_3(E_e) + \frac{\vec{\sigma}_n \cdot \vec{p}_e}{E_e} \frac{\vec{p}_e \cdot \vec{p}_\nu}{E_e E_\nu} C_4(E_e) + \frac{\vec{\sigma}_n \cdot \vec{p}_\nu}{E_\nu} C_5(E_e) + \frac{\vec{\sigma}_n \cdot \vec{p}_\nu}{E_\nu} \frac{\vec{p}_e \cdot \vec{p}_\nu}{E_e E_\nu} C_6(E_e) \right\}, \quad (5) \end{aligned}$$

where the coefficients  $C_i(E_e)$  are known functions of the same parameters:  $\lambda$ , recoil corrections, and radiative corrections. The functions  $C_1(E_e)/C_0(E_e)$ ,  $C_3(E_e)/C_0(E_e)$ , and  $C_5(E_e)/C_0(E_e)$  transform into coefficients  $a$ ,  $A$ , and  $B$  if recoil and radiative corrections are neglected.

Because all of the coefficients  $C_i(E_e)$  are functions of the same variables one can see that measurements of all the angular correlation coefficients in neutron  $\beta$ -decay in one (the same) experimental environment is the best way to obtain reliable values of the parameters  $\lambda$  and  $V_{ud}$ . This is also the best way to search for new physics which will manifest itself by a possible deviation of experimental results from the complete theoretical descriptions. Moreover, the complete measurement of the

Table 1: Statistical sensitivity factors of the standard experiments for different types of interactions from new physics.

Interactions	$a$	$A$	$B$
$\bar{a}_{LL}$	2.21	2.86	0.39
$\bar{a}_{LR}$	0.75	0.625	1.2
$\bar{a}_{RL}$	151	224	35.7
$\bar{a}_{RR}$	1000	1030	357
$\bar{A}_{RL}$	860	862	1000
$\bar{A}_{RR}$	860	862	1000

Table 2: Possible manifestations of new physics

Model	L-R	Exotic Fermion	Lepto Quark	Contact Interactions	SUSY	Higgs
$\bar{a}_{RL}$	0.067	0.042				
$\bar{a}_{RR}$	0.0075		0.01			
$\bar{A}_{LL} + \bar{A}_{LR}$				0.01	$7.5 \times 10^{-4}$	$3 \times 10^{-6}$
$\bar{A}_{RR} + \bar{A}_{RL}$				0.1		
$-\bar{A}_{LL} + \bar{A}_{LR}$			$3 \times 10^{-6}$			
$\bar{A}_{RR} - \bar{A}_{RL}$			$4 \times 10^{-4}$			

angular correlations gives the opportunity to tune the sensitivity of the experiment to a particular model related to new physics. As it is shown in [21], different models have different sensitivities to parameters of neutron decay rate. To illustrate this we can estimate a statistical sensitivity factor  $K$  for the parameter  $q$  related to new physics as

$$K = \sigma_q \cdot \sqrt{N}, \quad (6)$$

where

$$K^{-2} = \frac{\int w(\vec{x}) \left( \frac{1}{w(\vec{x})} \frac{\partial w(\vec{x})}{\partial q} \right)^2 d\vec{x}}{\int w(\vec{x}) d\vec{x}}. \quad (7)$$

Here  $w(\vec{x})$  is a distribution function of measurable parameters  $\vec{x}$ .  $N$  is a number of counts in the experiment, and  $\sigma_q$  is a variance (standard deviation) for the parameter  $q$ . For the purposes of simple comparison of the statistical sensitivity factors we assume that all  $\bar{a}_{jl}$  and  $\bar{A}_{jl}$  parameter have the same values:  $\bar{a}_{jl} = 0.001$  and  $\bar{A}_{jl} = 0.001$ . Then, the corresponding statistical sensitivity factors for the angular coefficients are shown in the table 1, which demonstrates relative resolutions or discovery potentials of different angular correlations to new physics. The real estimates for the  $\bar{a}_{jl}$  and  $\bar{A}_{jl}$  parameters are not as 0.001, used in the table 1, but vary in a wide range from 0.07 to  $10^{-6}$  (see table 2 and [18], for the comprehensive analysis). The comparison of these two tables can give a rough estimate of the statistical sensitivity factors for particular models and experiments. The relative contribution to the energy spectra corresponding to the  $a$ ,  $A$  and  $B$  correlations due to new physics, related to the  $\bar{a}_{RL}$  parameter, are shown in figures (1), (2), and (3). (The graphs on the figures are normalized by the total spectrum for each correlation with the assumption that new physics parameters have values of 0.001.) One can see that these contributions due to the  $\bar{a}_{RL}$  parameter have different shapes and positions of maxima. This allows fine tuning in the search for a particular model beyond the Standard one in our experiment.

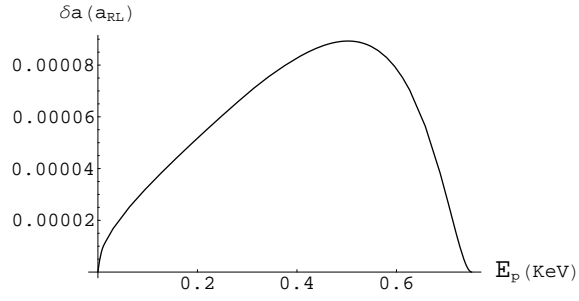


Figure 1: Manifestation of  $a_{RL}$ -type interactions  $a$  coefficient.

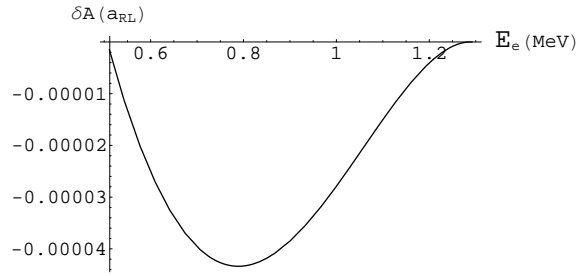


Figure 2: Manifestation of  $a_{RL}$ -type interactions  $A$  coefficient.

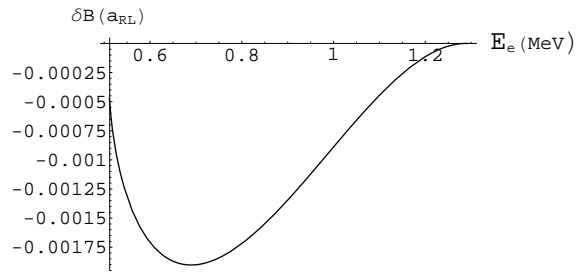


Figure 3: Manifestation of  $a_{RL}$ -type interactions  $B$  coefficient.

Previous experiments on determinations of  $\lambda$  in neutron decay have focused on measuring only one parameter, mostly  $A$ . Also these experiments have been limited in precision primarily by two effects: large backgrounds and uncertainty in neutron polarization. The  $abBA$  approach addresses the first of these limitations by observing coincidences between the decay protons and electrons in high-quality silicon detectors, significantly reducing the background. It also decreases the uncertainty in neutron polarization by the methods described later in this proposal. However, the revolutionary advantage of the  $abBA$  experiment as a new approach is the possibility to measure not independent angular correlation coefficients (even in one apparatus) but rather the possibility for the unambiguous determination of the essential parameters such as  $\lambda$ ,  $V_{ud}$ , and parameters required by new physics.

## 2 Technical Approach

The goal of the proposed work is the accurate measurement of *all* of the  $T$ -even neutron beta decay correlation coefficients ( $a$ ,  $b$ ,  $A$ , and  $B$ ) that do not require the determination of decay product polarization. A measurement of these coefficients in a *single apparatus* provides a high degree of redundancy which will allow multiple cross-checks of possible systematic effects as well as the extraction of theoretically important quantities (such as  $\lambda$ , or non-standard coupling constants) in a highly over-constrained way.

We propose to perform these measurements in two phases. The first phase will observe the decay of unpolarized neutrons and is being proposed as a separate experiment to measure the correlations  $a$  and  $b$ . (See the  $Nab$  letter of intent for more information.) The second phase of the measurement, in which the use of polarized neutrons will allow the determination of  $a$ ,  $b$ ,  $A$ , and  $B$  is addressed by this letter of intent. This set of measurements will provide an extremely robust, and even more accurate determination of  $\lambda$ , as well as a range of new tests of physics beyond the Standard Model.

There are three main components to our apparatus: 1) the decay spectrometer, 2) the neutron polarizer, and 3) the neutron source. The decay spectrometer is similar in both experiments although field uniformity constraints are significantly more severe for the  $abBA$  experiment than for the measurement of  $a$ . The neutron polarizer will be used only for this ( $abBA$ ) experiment.

### 2.1 Decay Spectrometer

The spectrometer is a highly efficient,  $4\pi$  charged particle detector that identifies a decay event by a delayed coincidence between a “fast” electron (TOF  $\approx 10$  ns) and a slow proton (TOF on the order of  $3 - 30 \mu\text{s}$ ). A schematic of the spectrometer is shown in figure 4.

The neutron beam passes through the decay volume of the spectrometer transverse to the magnetic field. In the decay region there is a strong, homogeneous magnetic field ( $\sim 4$  T) and the decay particles drift along the magnetic field lines with cyclotron orbit radii that will depend on their energies but will typically be on the order of a millimeter. (Note that although the characteristic energies of the protons and electrons differ by three orders of magnitude, their momenta, and thus their cyclotron radii have comparable scales.) Because the decay region is well within the tubular HV electrode, the electric field in the decay region is very small ( $< 1$  mV/cm).

As the particles drift from the decay region they pass through a region where the magnetic field decreases to  $\sim 1$  T. While this is a significant change in the magnetic field, in the frame of the decay particle, the change is slow compared with the cyclotron frequency so the charged particle transport is “adiabatic.” This implies that as the cyclotron radius increases, the particle’s transverse component

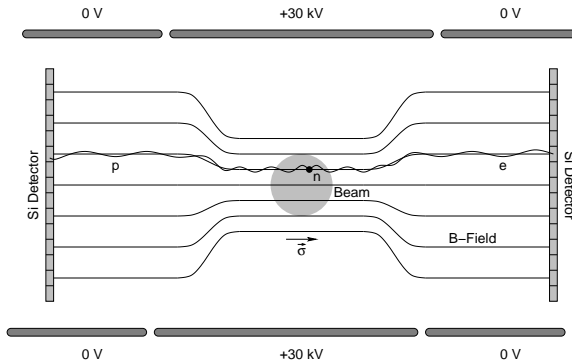


Figure 4: The conceptual design for the spectrometer showing the most important elements (not to scale). The beam direction is into the page.

of momentum is reduced, and the axial component is increased. This “longitudinalization” of the electron momentum greatly reduces the number of electrons that are Penning trapped and provides for 100% acceptance of electrons with total energy above 54 keV. The “longitudinalization” of the electron momentum also implies that the electrons will hit the silicon detector more normal to the surface than they would otherwise. This reduces the probability of backscattering. We also note that this field expansion also serves a critical function in the identification of backscattered events.

As shown in figure 5, the magnetic field expansion lies within the region where the electric potential is constant. After leaving the field expansion region the decay particles enter a region of relatively strong electric field (*i.e.* at this point they are near the end of the tubular HV electrode). In this region the protons (which initially have an energy  $\leq 750$  eV) are accelerated to an energy of  $\sim 30$  keV. At this energy the protons can be detected well above the noise in the silicon detector. The electrons that exit the HV electrode will, of course, lose this much energy. However, *every* electron that arrives at the silicon detector will have its energy reduced by an amount that corresponds *exactly* to the acceleration potential. Of course, some low energy electrons will be Penning “trapped” and not exit from the HV electrode. However, as noted above, the presence of the magnetic expansion ensures that every electron with a total energy that exceeds a threshold of 54 keV for the 4:1 field expansion and a 30 kV potential will reach a detector. Thus the electron spectrum above this threshold will exactly reflect the decay spectrum with only a fixed (and precisely known) offset.

Because the decay particles follow helical cyclotron orbits around the magnetic field line that passes through the location of the decay, they will hit a detector within two cyclotron radii (typically  $\leq 1$  cm) of the point where that flux line passes through the detector. If both the decay electron and proton go toward the same detector, they will hit within  $\sim 1$  cm of each other. If the electron and proton go toward different detectors, they will both hit close to “conjugate” points on the two detectors. This fact is quite useful and we exploit it by using a pixelated silicon detector with a pixel size of about  $1 \text{ cm}^2$ .

With such pixelation, a “true” coincidence can only occur in the same pixel, in adjacent pixels, or in conjugate pixels on the two detectors. This greatly reduces the probability of a false coincidence. This procedure also provides a number of redundant methods by which this small false coincidence background can be accurately measured. In addition to the usual procedures involving the addition of time delays, one can look for false coincidences in non-adjacent detectors. Finally we note that

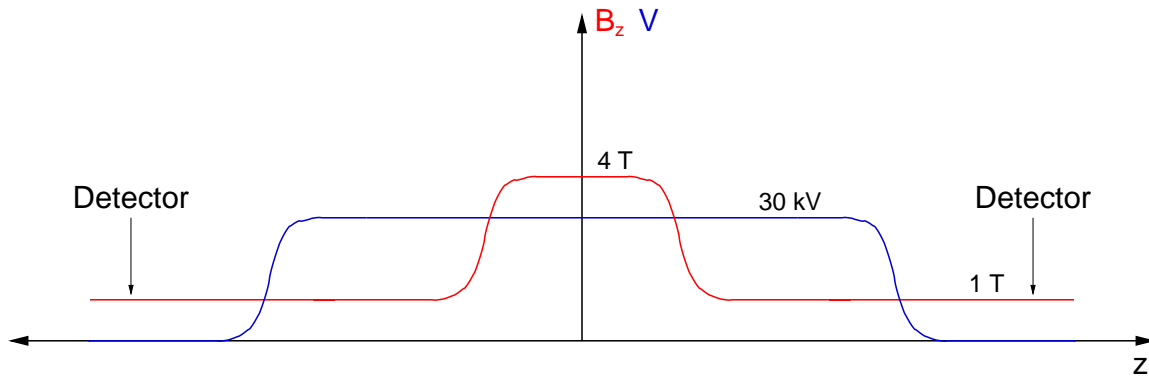


Figure 5: Configuration of the electric potential and magnetic field along the spectrometer axis, not to scale.

the combination of the high magnetic field and pixelated detector provides a virtual (*i.e.* aperture free) collimation of the decay particles. Only those neutron decays which occur on a magnetic field line which passes through an active detector pixel are observed. Thus, the observed decay volume is actively limited without the requirement of passive collimation. The acceptance of each detector is thus well-defined (a limiting systematic error in previous experiments).

If a decay electron stops entirely in a detector, its energy is either entirely deposited in a single pixel, or is shared between adjacent pixels. Each time there is a candidate event, the charge collected in every pixel that indicates an energy deposit above the noise threshold will be saved. A “real” event will show an energy deposit in only one, two, or three pixels (for hexagonal tiling). If an electron is backscattered from the Si (probability of  $\sim 20\%$ ) it will either be reflected back (probability  $\sim 85\%$ ) to the same (or adjacent) pixel by the  $\Theta$ -pinch magnetic mirror, or it will escape (probability  $\sim 15\%$ ) and strike the conjugate pixel on the opposite detector. Summing over adjacent cells in the same and conjugate detector gives the total electron energy.

Approximately 97% of the decay electrons deposit all of their energy in the first detector that they hit, either by stopping, or by backscattering and being reflected by the  $\Theta$ -pinch. For such electrons it is trivial to determine the initial direction (up-down) of the decay electron. The remaining 3% will split their energy between the two detectors. To determine the initial electron direction one must be able to determine which detector was “hit” first. This implies that the detectors require a time resolution comparable to the electron time-of-flight between the two detectors (typically a few to several ns).

Decay protons with  $\sim 30$  keV of energy are detected with high efficiency in the first detector they hit (The probability for back scattering of protons is of order  $\leq 1\%$  and the effects of proton backscattering are negligible. Note that the energy deposit for all proton hits will be essentially the same (the variation in initial energies of  $\sim 100$ 's of eV is below the detector resolution of  $\sim 3$ –5 keV). Thus, while the energy deposited by the protons is much smaller than electron, a true proton event is identifiable by a nearly unique energy signal.

Because the decay region is in an electric field-free region, the proton initially drifts along the magnetic field lines with its original axial momentum. After this drift, the proton momentum is longitudinalized by the field expansion and the proton is then accelerated to  $\sim 30$  keV. After

acceleration the proton very quickly hits the silicon detector. The magnet and electrode structure are designed so that the flight time in the field free region is much greater than the time of flight after longitudinalization and acceleration. The total proton time of flight will be approximately proportional to  $1/p_z$ , where  $p_z$  is the axial component of the proton's initial momentum. Thus the apparatus serves as simple proton spectrometer. The resolution of this spectrometer is limited to 10% at higher proton velocities increasing to 25% at lower velocities (as determined by simulations) by effects due to the longitudinalization. Nonetheless, even this rather rough resolution provides important information about the kinematics of the decay. The inclusion of this information increases the overall sensitivity of the measurement of  $a$  by a factor of  $\sim 2.3$ .

To summarize, using coincident detection of decay electrons and protons, the spectrometer provides, with high efficiency and low (well understood) background, the following reconstruction of each decay event:

1. Total electron energy.
2. Sign of axial component of the electron momentum (electron up or down?)
3. Sign of axial component of the proton momentum (proton up or down?)
4. Magnitude the axial component of the proton momentum.

## 2.2 Charged-Particle Detectors

The charged-particle detectors are located at either end of the spectrometer, with each detecting the electrons and protons from decay events over one half of  $4\pi$ . The requirements on the detectors are rather stringent, including:

1. Accurate calorimetry for electrons with energies 50–800 keV.
2. Detection of protons with energies of 30 keV (*i.e.* very thin and uniform surface dead layer).
3. Large area ( $\approx 100 \text{ cm}^2$ ).
4. Position sensitivity.
5. Small and position-independent reflection probability for electrons.
6. Accurate (few nanosecond) timing.
7. High and stable electron detection efficiency.
8. Position-independent detection efficiency.
9. Energy-independent detection efficiency.

These requirements are met with large-area, thin-window, ion-implanted silicon detectors. The reference detector design is made from a 15 cm diameter, 2 mm thick silicon wafer. The silicon is bulk  $n$ -type, with a  $p$ -type implant on the front surface to form the diode junction. The front surface is essentially featureless, with a fine aluminum grid covering 0.5% of the active area. The back surface is metalized with a pattern of 121 hexagons to segment the charge collection, providing position resolution. The hexagonal cells have sides measuring 5.7 mm and the total active area

of the detector is approximately  $100 \text{ cm}^2$ . The detector is mounted to a ceramic carrier, allowing for cooling to cryogenic temperatures. A PC board is mounted behind the ceramic with the front-end electronics (FET plus feedback components) and bias circuitry. The detectors are cooled to approximately 100 K. Cooling the detectors both improves the energy resolution and increases the carrier velocities, resulting in improved timing resolution.

### 2.3 Neutron Polarimetry

One of the largest systematic uncertainties in previous measurements of neutron polarization-dependent observables has been knowledge of the neutron polarization. The neutron beams were polarized by supermirror polarizer devices, which reflect (or transmit) one neutron polarization state using magnetized supermirror surfaces. The resulting neutron beam polarization, while quite high, is energy and angle dependent and requires auxiliary experiments to determine accurately. We will use a polarized  $^3\text{He}$  spin filter to polarize the neutron beam. This technique allows for continuous, accurate, and *in situ* determination of the neutron beam polarization.

In this approach, the neutron beam is polarized by passage through a gas of polarized  $^3\text{He}$ . A cell containing  $^3\text{He}$  gas and a small amount of rubidium is polarized by first polarizing the Rb with circularly polarized laser light. Spin exchange between Rb and  $^3\text{He}$  transfers the polarization. Because the cross section for neutron absorption on  $^3\text{He}$  is strongly spin-dependent (10.6 kbarn for spins anti-parallel and 3 barn for spins parallel at 25.3 meV), the polarized  $^3\text{He}$  acts as a spin filter, preferentially transmitting neutrons of one spin state. This technique has been used by us and others in experiments requiring polarized neutron beams. In addition, the  $n$ - $^3\text{He}$  cross section scales very accurately with the inverse of the neutron velocity [22]. For any neutron energy, there is then a parametric relation between neutron polarization and neutron time-of-flight  $P_n = \tanh(t/\tau)$  where  $\tau = P_3 L / n_3 \sigma_v v$ , with the  $^3\text{He}$  polarization and thickness given by  $P_3$  and  $n_3$ , the flight path length given by  $L$ , and the  $n$ - $^3\text{He}$  cross section at neutron velocity  $v$  given by  $\sigma_v$ . A similar relationship also holds for the neutron transmission through a polarized  $^3\text{He}$  gas. This relationship has been used to measure absolute neutron polarization to an accuracy of 0.3% for neutron energies from 40 meV to 10 eV [23] in a dedicated measurement which was statistics limited. Present knowledge of the  $n$ - $^3\text{He}$  interaction indicates the relationship holds to at least the  $10^{-4}$  level and can thus be used as the basis for a precision neutron polarimetry technique at cold ( $< 25 \text{ meV}$ ) neutron energies. In fact, detailed knowledge of  $\tau$  is not required for precision neutron polarimetry in this experiment. Because the neutron decay parameters are independent of neutron energy, the time-of-flight dependence of the polarization-dependent asymmetries due to  $A$  and  $B$  comes only from time-of-flight dependence of  $P_n$ , which is described above. Analysis of these asymmetries as a function of neutron time-of-flight allows extraction of both the decay parameters  $A$  and  $B$ , and the parameter  $\tau$ , which completely characterizes the neutron polarization.

Work is continuing on developing this technique for the *abBA* experiment. The collaboration is pursuing development of spin filters with improved properties, including increased  $^3\text{He}$  polarization and improved cell geometry. It is desirable to have the largest possible  $^3\text{He}$  polarization, to maximize both neutron polarization and transmission. Maximizing  $P_n$  not only maximizes the statistical figure-of-merit for polarized neutron experiments, it also minimizes the relative uncertainty in  $P_n$  and thus its contribution to the overall systematic uncertainty. Curved or uneven glass walls complicate the determination of neutron absorption in the glass walls of the cell, making flat entrance and exit windows desirable. Such cells also have the advantage of making the  $^3\text{He}$  thickness and thus neutron polarization constant across the beam profile. We have obtained 75%  $^3\text{He}$  polarization

in long-lifetime blown-glass cells, but the shorter lifetimes typical of flat-windowed cells (about 80 hours) presently limit the polarization to 65% in large cells. With improved lifetimes and/or more efficient optical pumping using rubidium-potassium mixtures, it may be possible to obtain 75% in flat-windowed cells. Frequency-narrowed lasers for polarizing these cells have shown great promise for increasing the  $^3\text{He}$  polarization.

## 2.4 Statistical Sensitivity

We have calculated the relation between neutron counting statistics and statistical precision for each of the correlations. For an assumed average neutron polarization of 80%, the statistical sensitivity factors are:

$$\sigma_a\sqrt{N} = 4.7, \quad (8)$$

$$\sigma_A\sqrt{N} = 3.1, \quad (9)$$

$$\sigma_B\sqrt{N} = 2.3, \quad (10)$$

It is important to recognize that these measurements are slightly correlated. Including this correlation and assuming the Standard Model dependences on  $\lambda$ , one obtains an overall sensitivity factor of:

$$\sigma_\lambda\sqrt{N} = 7.4. \quad (11)$$

With the anticipated count rate of  $\sim 180$  polarized neutron decays per second at the SNS, one will obtain  $\sim 1.5 \times 10^9$  decays in 100 days of data collection. This implies the following statistical errors:

$$\begin{aligned} \sigma_a &\approx 1.2 \times 10^{-4} & \sigma_a/a &\approx 1.2 \times 10^{-3} \\ \sigma_A &\approx 0.8 \times 10^{-4} & \sigma_A/A &\approx 0.8 \times 10^{-3} \\ \sigma_B &\approx 0.6 \times 10^{-5} & \sigma_B/B &\approx 0.6 \times 10^{-3} \end{aligned} \quad (12)$$

These statistical errors are all substantially less than the *total errors* quoted by the PDG. The expected uncertainty for  $\lambda = g_A/g_V$  is then:

$$\sigma_\lambda \approx 1.8 \times 10^{-4}, \quad (13)$$

$$\sigma_\lambda/\lambda \approx 1.5 \times 10^{-4}. \quad (14)$$

We conclude from this analysis that, not only do we expect that counting time will not be a serious issue, but also that the statistical reach of the experiment will allow the opportunity to fully explore possible systematic effects.

## 2.5 Systematic Effects

The major systematic effects can be divided into four categories: neutron polarimetry, detector backgrounds, interaction of the charged particles with electromagnetic fields, and interaction of the charged particles with the detector. The first two categories have been discussed elsewhere in this document. This section describes the primary remaining systematic effects.

### 2.5.1 Interaction of Charged Particles with Electromagnetic Fields

**Reflection of charged particles by magnetic field gradients** If an electron or proton encounters an increasing magnetic field along its trajectory, it can be reflected, causing it to arrive at the ‘wrong’ detector. This effect is only important in the central region of the spectrometer, before the particle trajectories are longitudinalized. In particular, it imposes a homogeneity requirement on the magnetic field inside the fiducial decay volume. It is possible to design a spectrometer magnetic that reduces this effect to the  $10^{-3}$  level.

**Proton time-of-flight cutoff** The time-of-flight of a proton from the decay event to a detector is dominated by the time required to travel to the electric field gradient where it is accelerated to 30 kV. In this approximation, the time depends upon the  $z$  component of the proton velocity and the the distribution of arrival times can be shown to be proportional to  $1/t^2$ . Since the time window for electron-proton coincidence must be finite, some protons will not be observed within this window. The fraction lost depends upon the spectrometer geometry and coincidence window. We have estimated the loss to be  $\approx 1\%$  for a realistic geometry and a 100  $\mu\text{s}$  coincidence window.

### 2.5.2 Interaction of Charged Particles with Detectors

**Electron backscattering** Electrons striking a detector reflect from the surface with a fairly high probability. This probability is both energy and angle dependent. Most of the the backscattered electrons and the reflected by the high central magnetic field of the spectrometer, returning to the correct detector, but a few percent subsequently strike the second detector. In these cases, the timing resolution of the detectors must be sufficient to resolve which detector was hit first, to correctly identify the initial direction of the electron. In some fraction of these events, the energy deposited in one detector will be below the detection threshold. Careful modeling of this process is required and study of the effect as a function of detector threshold will be performed.

**Detector efficiency** Several mechanisms exist for particles to be missed by the detectors. A few, such as proton time-of-flight cutoff and electron backscattering, have been discussed previously. In addition, there are other mechanisms. Approximately 0.5% of protons strike the aluminum detector grid, losing enough energy that they are not detectable. Fortunately, because of the 30 kV accelerating potential, this loss is independent of the proton momentum, and therefore does not bias the measurement. Electrons falling below the detection threshold, however are more problematic. For this reason, it is important to reduce detector noise as much as possible.

**Detector energy resolution** Because extraction of the neutron decay parameters requires knowledge of the electron energy, it is important to have a good energy resolution. Contributing to this resolution is intrinsic detector noise, charge-sharing between adjacent pixels, and bremsstrahlung by the electrons in the silicon. We believe that an energy resolution of a few keV can be achieved.

### 3 Beam Time Requirement

Based on the counting rate estimate described above, approximately 100 days of live data collection are required to achieve the statistical goals of this letter of intent. In addition, beam time will be required for systematic studies, estimated at approximately 250 days. Before data collection begins, an extensive period of engineering runs will be required, estimated at 100 days. The total estimate for beam time is 450 days.

### 4 Research and Development

Research and development is continuing in several areas. Detector development is ongoing, with the first full-size prototypes expected in fall 2005. DAQ electronics development is in progress. Demonstration of precision neutron polarimetry and associated techniques is planned for the FP12 cold neutron beam at LANL for 2006–2008. Collaborative work on improving polarizer performance continues. Modeling of charged-particle trajectories in the spectrometer continues to advance. Preliminary design of the experiment will advance in parallel with these efforts.

### 5 Construction and Commissioning

While the precise schedule for construction and commissioning will depend upon decisions made by the funding agencies, table 3 lists preliminary milestones.

Finish R&D	2008
Begin Construction	2008
Finish Construction	2009
Begin Commissioning	2010
Begin Operations	2011

Table 3: Preliminary milestones for the construction and commissioning of the *abBA* experiment.

### 6 Facility Requirements

#### 6.1 Facility Modifications

Beyond the requirements listed below, the only significant facility modification required may be concrete coring at the spectrometer location to accommodate the lower arm of the spectrometer, depending upon the final spectrometer dimensions.

#### 6.2 Radiation Shielding

Because there is no target in the experiment, radiation shielding requirements are modest, except for the beam dump. Vacuum windows through which the beam passes may require shielding for the scattered neutrons. The beam dump needs to be located a few meters downstream of the spectrometer to reduce backgrounds.

### 6.3 Magnetic Shielding

The spectrometer magnet will be vertical and will contain an integral iron cylinder for flux return. Magnetic fields outside of this shield in the axial direction will be less than 100 G. Fields at the top and bottom of the spectrometer will be higher. Additional magnetic shielding will be necessary to meet facility requirements. It may be possible to incorporate the magnetic shielding into the radiation shielding package.

### 6.4 Utilities

Detailed utilities will be coordinated with ORNL staff. Approximately 75 kVA of 120 V single phase and 208 V three-phase electrical power (of which approximately 15 kVA has an isolated ground on a separate transformer) will be required. Modest capacity for chilled water, required for cryocompressors will be needed, as well as house air for actuating valves. Provision for inert gas in cylinders is required and a vent line for vacuum pumps. Crane access will be required for spectrometer maintenance.

## References

- [1] I. Towner and J. Hardy, Phys. Rev. C **66**, 035501 (2002).
- [2] S. Dzhosyuk *et al.*, J. Res. Natl. Inst. Stand. Technol. (2005).
- [3] W. Wilburn, J. Bowman, G. Mitchell, J. O'Donnell, S. Penttilä, and P.-N. Seo, J. Res. Natl. Inst. Stand. Technol. (2005), in press.
- [4] P. D. Group, Phys. Rev. D **66**, 010001 (2002).
- [5] G. Isidori (2003), arXiv:hep-ph/0311044.
- [6] A. Sirlin (2003), arXiv:hep-ph/0309187.
- [7] H. Abele, Nucl. Instrum. Methods A **440**, 499 (2000).
- [8] B. Holstein and S. Treiman, Phys. Rev. D **16**, 2369 (1977).
- [9] J. Deutsch, in *Fundamental Symmetries and Nuclear Structure*, edited by J. Ginocchio and S. Rosen (World Scientific, Singapore, 1989), p. 36.
- [10] P. Herczeg, in *Fundamental Physics with Pulsed Neutron Beams*, edited by C. Gould, G. Greene, F. Plasil, and W. Snow (World Scientific, Singapore, 2001), p. 64.
- [11] B. Yerozolimsky, Nucl. Instrum. Methods A **440**, 491 (2000).
- [12] W. Marciano, Nucl. Phys. **B116**, 437 (2003).
- [13] V. Cirigliano, G. Ecker, M. Eidemuller, A. Pich, and J. Portoles (2004), arXiv:hep-ph/0404004.
- [14] V. Cirigliano, J. Res. Natl. Inst. Stand. Technol. **110** (2005).
- [15] J. Jackson, S. Treiman, and H. Wyld Jr., Phys. Rev. **106**, 517 (1957).

- [16] A. Sirlin, Phys. Rev. **164**, 1767 (1967).
- [17] V. Gudkov, J. Neut. Res. **13**, 39 (2005).
- [18] P. Herczeg, Prog. Part. Nucl. Phys. **46**, 413 (2001).
- [19] H. F. S. Ando, V. Gudkov, K. Kubodera, F. Myhrer, S. Nakamura, and T. Sato, Phys. Lett. **B595**, 250 (2004).
- [20] V. Gudkov, K. Kubodera, and F. Myhrer, J. Res. Natl. Inst. Stand. Technol. (2005).
- [21] J. Calarco, G. Green, and V. Gudkov, in Preparation.
- [22] C. Keith, Z. C. D. Rich, W. Snow, J. Bowman, S. Penttilä, D. Smith, M. Leuschner, V. Pomeroy, G. Jones, and E. Sharapov, Phys. Rev. C **69**, 034005 (2004).
- [23] D. Rich, J. Bowman, B. Crawford, P. Delheij, M. Espy, T. Haseyama, G. Jones, C. Keith, J. Knudson, M. Leuschner, A. Masaike, Y. Matsuda, *et al.*, Nucl. Instrum. Methods A **481**, 431 (2002).